University of Claude Bernard Lyon 1

Polytech Lyon

Estimation of Image-Derived Arterial Input Function in Brain PET Imaging: Application to Modeling PET Dynamics of Glucose Metabolism in Patients with Impaired Consciousness

By Sepand Ali Madad Soltani

Master's Thesis Report

Supervised by Inés Mérida and Nicolas Costes

Academic Advisor: Kevin Tse Ve Koon

November 2024 - January 2025

Abstract

Keywords: PET, Image-Derived, ...

Contents

Introduction

1.1 Positron Emission Tomography

Positron Emission Tomography (PET) is a functional imaging technique widely used in clinical and research settings to monitor physiological processes. In PET, a biologically active molecule is labeled with a positron-emitting radioisotope, known as radiotracer and then injected into the body. As the radiotracer accumulates in target tissues, its radioactive decay produces positrons, which interact with electrons to emit pairs of gamma photons in nearly opposite directions. These photons are detected by the PET scanner, and through image reconstruction algorithms, a three-dimensional representation of tracer distribution is generated. This imaging modality allows for the investigation of metabolic changes, receptor binding, and other biochemical processes, providing invaluable information in oncology, neurology, cardiology, and other fields.

There are two main methods of acquiring PETs. Dynamic and static imaging. Static PET involves acquiring a single scan after the radiotracer injection. This single snapshot offers a powerful yet simplified view of tracer distribution. The common quantification metric in static imaging is the Standardized Uptake Value (SUV). The SUV normalizes tissue uptake by injected dose and patient weight, allowing a semi-quantitative comparison of tracer accumulation across different tissues or over time. [**TODO**] Due to its simplicity, static PET is widely used in clinical settings but it also comes with limitations. Because it reflects just one time point, the SUV cannot capture the temporal dynamics of how a tracer is taken up and cleared, and various physiological factors can influence its measurements reducing its accuracy.

Dynamic PET provides a more comprehensive view of the radiotracer kinetics by acquiring a series of images over a period of time-ranging from few minutes to more than an hour depending on the tracer type-immediately following tracer administration. Instead of a single snapshot, dynamic imaging produces time-activity curves (TAC), presenting how tracer concentration in each tissue changes over the entire scanning period. This allows for measuring physiological parameters such as tracer rate of influx (K_i), volume of distribution (V_T), and rates of phosphorylation and dephosphorylation. This greater depth of information is especially valuable in research settings where....

1.2 Compartmental Model

To measure these parameters of interest, kinetic modeling must be carried out. Number of graphical models (e.g. Logan [**TODO**] and Patlak [**TODO**]) have been proposed but compartmental modeling is the most popular and is considered as the most accurate of kinetic modeling. Compartment modeling is a mathematical framework where the distribution and kinetics of a radiotracer are described by dividing the system into distinct "compartments," each representing pools of tracer in blood or organs that behave in a uniform or homogeneous way and interact with other compartments. Interaction can be one way or two way with other compartments, meaning the tracer can either enter and leave or just enter the compartment.

Here, we will focus on two-tissue compartment model (2TCM) or also known as three compartment model in series mode with FDG as the tracer. It consists of one compartment or one tissue for the free tracer $C_F(t)$ and another for the receptor-bounded tracer $C_B(t)$, plus an external compartment that represents the concentration of the tracer in the plasma or the blood which is known as the input function $C_P(t)$.

The tracer kinetics is governed by a series of first-order differntial equations where the exchange rate between the compartments is considered as constants:

$$\frac{dC_F(t)}{dt} = K_1\, C_P(t) \;-\; \big(k_2 + k_3\big) C_F(t) \;+\; k_4 C_B(t)\,, \tag{1.1}$$

$$\frac{dC_B(t)}{dt} = k_3\, C_F(t) \;-\; k_4\, C_B(t), \tag{1.2}$$

where K_1, k_2, k_3, k_4 are the constant rates.

It's considered that once FDG is phosphorylated (bounded), there is little to no dephosphorylation back to the free compartment (unbounding). Meaning, we can can consider $k_4 = 0$ [**TODO**]. This is why this variant is called the irreversible two-tissue compartment model. Thus Equation (1.1) and (1.2) simplifiy to

$$\frac{dC_F(t)}{dt} = K_1\, C_P(t) \;-\; \big(k_2 + k_3\big) C_F(t)\,, \tag{1.3}$$

$$\frac{dC_B(t)}{dt} = k_3\, C_F(t), \tag{1.4}$$

The total tissue and blood concentration $C_T(t)$ that is measured in PET (i.e. the PET signal) is the

$$C_T(t) \;=\; C_F(t) \;+\; C_B(t) \;+\; C_P(t). \tag{1.5}$$

The parameters K_1, k_2, k_3 can be estimated by fitting the model to the measured PET TACs, using the input function as $C_P(t)$. At the end, we can derive K_i or the influx rate

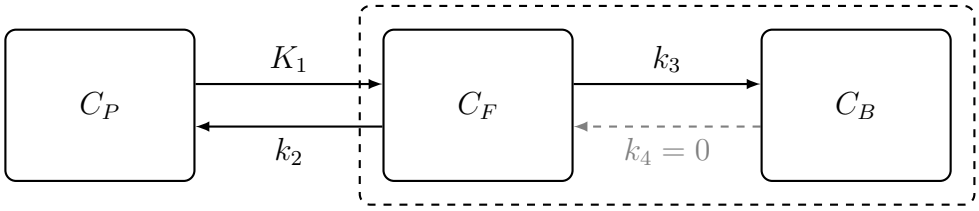

Figure 1.1: Schematic of the irreversible two-tissue compartment model (2TCM)

(trapping rate) of FDG in the tissue as

$$K_i = \frac{K_1 \times k_3}{k_2 + k_3} \tag{1.6}$$

FDG is an analog of glucose, not glucose itself. To convert the FDG trapping rate to the actual rate of glucose metabolism, the glucose concentration and the lumped constant is taken in to account.

$$\text{MR}_{glu}(\ \mu\text{mol/min/100g}) = \frac{[C]}{LC} \cdot K_i \tag{1.7}$$

where MR_{glu} is the metabolic rate of glucose, $[C]$ is the glucose concentration, and LC is the lumped constant.

1.3 Input Function

1.3.1 Arterial Input Function

Arterial input function (AIF) is considered the gold standard measure of deriving the input function. This is done by inserting an arterial catheter in to the patient and continously drawing blood sample and measuring its radiotracer concentration to obtain the blood TAC to be used in the quantification model. This procedure is invasive and causes discomfort for the patient which could subsequently discourage them from participating in future examinations. Moreover, this method is labour intensive and requires trained personnel to handle the patient and the measuring devices.

1.3.2 Image Derived Input Function

Image derived input function (IDIF) is proposed as an alternative non-invasive method of obtaining the input function. IDIF techniques typically involve identifying vascular structures or regions with high blood pool activity within the imaging field and extracting the input function from the PET image. Carotids are the largest arteries included in the limited filed of view (FOV) of brain PET with a diameter of about 5 mm which is comparable to a typical PET spatial resolution. So the extraction of the carotids directly from the PET would be impractical due the limited resolution of PET images and strong partial volume effect (PVE) present.

With the emergence of hybrid PET/MRI machines, simultaneous acquisition functional and anatomical data has became possible, with MRI providing high-resolution soft tissue contrast and PET capturing metabolic activity. Time-of-flight (TOF) MR angiography (MRA) provides high contrast in arteries which can be used for accurate segmentation of the carotids. Even with an accurate segmentation of the arteries, the input function derived by directly applying the mask on to the PET image would suffers from partial volume effects which need correction.

Irace et al. [1] proposed method for IDIF estimation by an MRA-driven carotids segmentation and a bayesian framework for incorporating prior knowledge in to a geometric transfer matrix method -a classical partial volume correction method. The aim here was to improve on this method and increase accuracy.

Materials and Methods

2.1 Dataset Description

We utilized a dataset of 56 comatose patients, aged between X and Y years, in which dynamic PET imaging was conducted 90 minutes using ^{18}FDG as the tr[illegible], with arterial blood sampling and TOF-MRA images acquired during the same session.

2.2 Carotid Segmentation

Since vessels appear as hypersignal in TOF-MRA, a high-intensity thresholding technique was employed. First, a threshold value was computed by selecting all nonzero intensity values and then determining the intensity level at the $(1 - 0.003)$ quantile (i.e., the 99.7th percentile) of these intensities. Only voxels exceeding this threshold and located outside the brain mask were retained. Next, a region-growing step was applied to refine the initial selection, ensuring that continuous vascular structures were captured as the final carotid mask.

In addition to arteries, venous structures and possible brain lesions may also appear as hypersignal and might be selected by the algorithm. To exclude them, a cuboid mask was defined in a reference image covering the neck area up to the bottom of the brain, where the carotid is most likely to appear. The MRA image was first registered to the reference image using an affine registeration technique (FSL FLIRT). Using the obtained affine matrix, the cuboid mask was first transformed and then applied to the MRA image before thresholding step to ensure the mentioned unwanted tissues will not effect the intensity histograms and do not get selected as carotid.

2.3 Partial Volume Correction

2.3.1 Geometric Transfer Matrix

Direct quantification with the IDIF extracted from the MRI mask of the carotid is impractical due to the strong Partial Volume Effects (PVE) in PET images. This however can be

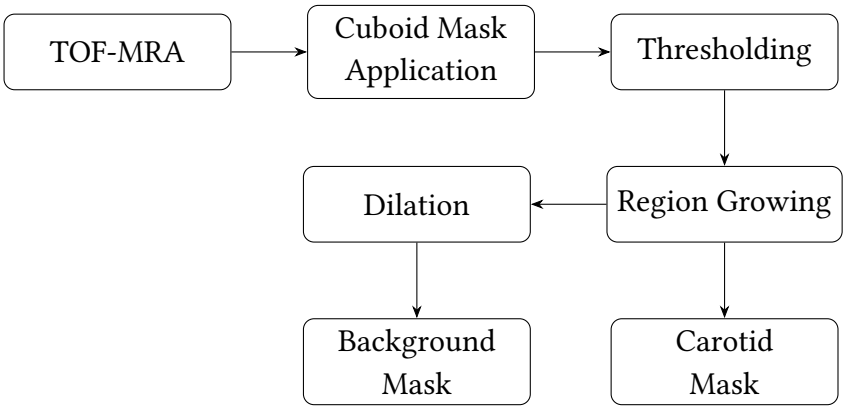

Figure 2.1: Carotid and background mask segmentation pipeline

corrected by the use of the Geometric Transfer Matrix (GTM) method. This method considers the observered TAC to be the linear combination of the true real value and the other effecting regions. Here we define two regions, the carotid and the background mask which was generated by dilating the carotid mask by 5 pixels and subtracting the voxels corresponding to the carotid mask.

$$\underbrace{\begin{bmatrix} T_c \\ T_{bg} \end{bmatrix}}_{\text{Observered}} = \underbrace{\begin{bmatrix} \omega_{c\to c} & \omega_{bg\to c} \\ \omega_{c\to bg} & \omega_{bg\to bg} \end{bmatrix}}_{\text{GTM}} \cdot \underbrace{\begin{bmatrix} T_{IF} \\ T_{tissue} \end{bmatrix}}_{\text{Unknown}}, \tag{2.1}$$

where $\omega_{n\to m}$ is the spill coefficient of region n onto region m, which is obtained by convolving the binary mask of region n with the system's point spread function and integrating the resulting intensity over region m, normalized by the total signal in region m. where

$$\omega_{n\to m} = \frac{\displaystyle\int_{\Omega_m} \big(h * \chi_n\big)(\mathbf{r})\, d\mathbf{r}}{\displaystyle\int_{\Omega_m} \big(h * \chi_m\big)(\mathbf{r})\, d\mathbf{r}}, \tag{2.2}$$

with χ_n and χ_m denoting the binary masks of regions n and m, respectively, h the system's point spread function, and Ω_m the spatial domain of region m.

T_c and T_{bg} are respectively the observered carotid and background TACs and T_{IF} and T_{tissue} are the real unknown TACs of the carotid (the input function) and the background tissue.

By inversing the GTM, this system of equations can be easily solved. However, the GTM being a low rank matrix makes the inversion sensitive to noise and biased on small regions such as the carotid.

2.3.2 Bayesian Geometric Transfer Matrix

To overcome challenges posed to GTM method, we utilized a Bayesian framework that jointly estimates the input function and tissue kinetics. For each subject, T_{IF} is modeled as a linear combination of a population mean and its principal components. These components are derived by performing principal component analysis (PCA) on a set of AIFs collected from the population. Specifically, for each subject, a subset of 10 random subjects is selected from the dataset—excluding the subject under study—to construct the PCA model.

$$T_{IF}(t) = \mu(t) + \theta_1 v_1(t) + \theta_2 v_2(t) + \theta_3 v_3(t), \tag{2.3}$$

where $\mu(t)$ is the population mean AIF, $v_i(t)$ are the principal components obtained from PCA, and θ_i are the subject-specific weighting coefficients.

The background TAC is then generated by convolving this modeled input function with an impulse response function (IRF) defined by a two-tissue compartment model [2].

$$T_{bg}(t) = T_{IF}(t) \circledast IRF(t; K_1, k_2, k_3), \tag{2.4}$$

where K_1, k_2, and k_3 are kinetic parameters of the two-tissue compartment and IRF is

$$IRF(t) = a_0 e^{-(k_2+k_3)t} + a_1 \text{ with } a_0 = \frac{K_1 k_2}{k_2 + k_3}, a_1 = \frac{K_1 k_3}{k_2 + k_3}. \tag{2.5}$$

Parameter estimation is performed using a Metropolis-within-Gibbs Markov Chain Monte Carlo (MCMC) sampler, which explores the posterior distribution of both the kinetic parameters and the PCA coefficients. In the Bayesian framework [1], all model parameters are collected into the vector Θ. The posterior distribution of Θ given the observed data $\mathcal{D}$ is expressed as

$$p(\Theta \mid \mathcal{D}) \propto p(\mathcal{D} \mid \Theta)\pi(\Theta), \tag{2.6}$$

where $p(\mathcal{D} \mid \Theta)$ is the likelihood function and $\pi(\Theta)$ is the prior distribution over the parameters $\Theta = (\theta_1, \theta_2, \theta_3, K_1, k_2, k_3)$. The maximum a posteriori (MAP) estimate of Θ is given by:

$$\hat{\Theta} = \arg\max_{\Theta} \left\{ \ln p(\mathcal{D} \mid \Theta) + \ln \pi(\Theta) \right\}. \tag{2.7}$$

2.4 Quantification

To accurately evaluate the performance of the estimated IDIF against the gold standard AIF, we performed absolute quantification using an irreversible two-tissue compartment model (2TCM) via non-linear fitting with the `fitk3` program from the TPCCLIB library developed at the Turku PET Centre [3]—applying the model fitting once with the IDIF and once with the AIF as the input function. The brain was segmented into regions of interest

(ROI) based on the Hammersmith brain atlas [**TODO**], and time-activity curves (TACs) were generated by averaging voxels over each ROI at every time point. The regional influx rate (K_i) was then calculated, from which the corresponding MR_{glu} values were derived.

2.5 Evaluation

The performance of the proposed IDIF estimation was first evaluated by computing the mean absolut error between the cumulative area under the curve (cAUC) of the estimated IDIF and the *true* AIF. cAUC was considered to be a more suitable metric since it provides an integrated measure of tracer exposure over time and is less sensitive to local fluctuations or noise in the curve compared to the directly comparing the TACs.

$$\text{cAUC}(t) = \int_0^t IF(\tau)\, d\tau, \tag{2.8}$$

where IF is the input function.

However, because the cAUC error does not fully capture the impact of IDIF deviations on kinetic parameters, absolute quantification was also performed to assess overall performance more accurately. The quantification program was run using both the IDIF and AIF as input functions, and the regional metabolic rate of glucose was compared between the two methods.

The mean absolute percentage error (MAPE) of the MR_{glu} in each ROI was calculated and then averaged across the entire dataset:

$$\text{Average MAPE}(\text{MR}_{\text{glu}}) = \frac{100\%}{N} \sum_{i=1}^{N} \left(\frac{1}{N_{\text{ROI}}} \sum_{j=1}^{N_{\text{ROI}}} \left| \frac{\text{MR}^{\text{IDIF}}_{\text{glu},ij} - \text{MR}^{\text{AIF}}_{\text{glu},ij}}{\text{MR}^{\text{AIF}}_{\text{glu},ij}} \right| \right). \tag{2.9}$$

Additionally, linear least-squares regression was performed between the regional MR_{glu} obtained by quantification with using AIF and IDIF for each subject. The coefficient of determination (R^2) and the regression slope (S) were obtained for each subject. The mean absolute errors (MAE) of these metrics across the dataset are given by

$$\text{MAE}(R^2) = \frac{1}{N} \sum_{i=1}^{N} \left| R_i^2 - 1 \right| \tag{2.10}$$

and

$$\text{MAE}(S) = \frac{1}{N} \sum_{i=1}^{N} \left| S_i - 1 \right|, \tag{2.11}$$

where R_i^2 and S_i denote the coefficient of determination and the regression slope for subject i, respectively.

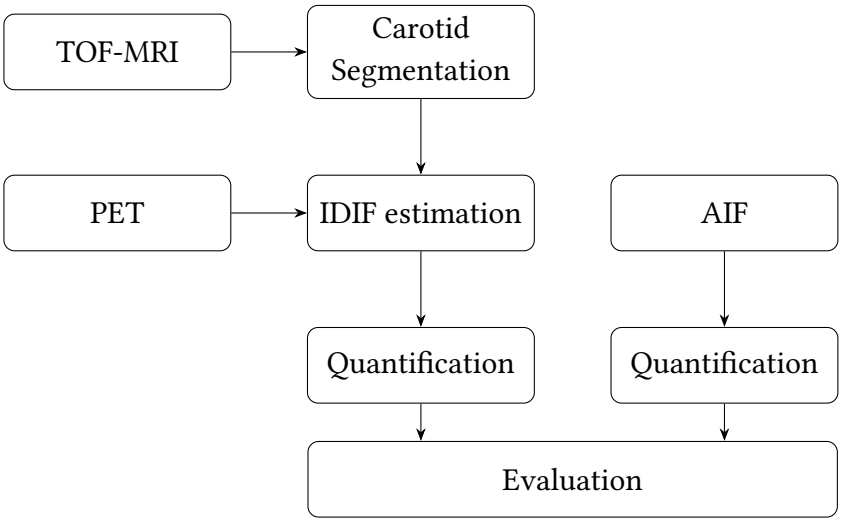

Figure 2.2: The IDIF estimation and evaluation pipeline

2.6 Implementation

The code was primarily implemented in Python, with some auxiliary components in Bash scripts. The underlying algorithm and implementation was originally developed by Irace et al. [1]. Building on this foundation, a number of improvements and additions were introduced to the code and the algorithm.

In the original carotid segmentation algorithm, the TOF-MRA image was smoothed to reduce noise. The purpose of this smoothing step was to attenuate noise; however, because carotids inherently exhibit high-frequency spatial features, the smoothing inadvertently blurred these critical details, ultimately reducing the accuracy of the segmentation. Hence, this step was removed.

In the adaptive thresholding step, all voxels, including those with zero intensity were originally included. This led to a significant imbalance in the intensity histograms, making the thresholding highly susceptible to variations in the number of slices and the effects of zero padding in the TOF-MRA image. Limiting to only nonzero voxels resulted in an immediate improvement in the final segmentation. Despite these improvements, some non-carotid tissues were inadvertently selected by the algorithm, hence the cuboid mask mentioned in Section 2.2 was introduced.

Significant improvements have been made to the overall code quality and performance. These include major bug fixes, streamlining the pipeline, multi-processing support, and the integration of evaluation metrics for individual subjects as well as for overall dataset performance.

Results

3.1 Segmentation

The proposed measures mentioned in Section 2.2 significantly improved carotid segmentation by excluding lesions and unwanted venous. As apparent by Figure 3.1, we can see the importance of the cuboid mask. Since the segmentation does not have a ground truth to be compared to, visual inspection of the segmentation showed promising results and lesions and venous were rarely selected by the algorithm. However, the algorithm became overly conservative. In some cases, even though no non-carotid tissues were selected, parts of the carotid structure were excluded. In other cases, the cuboid mask registration either failed entirely or was insufficiently accurate, resulting in the exclusion of parts of the carotid structure.

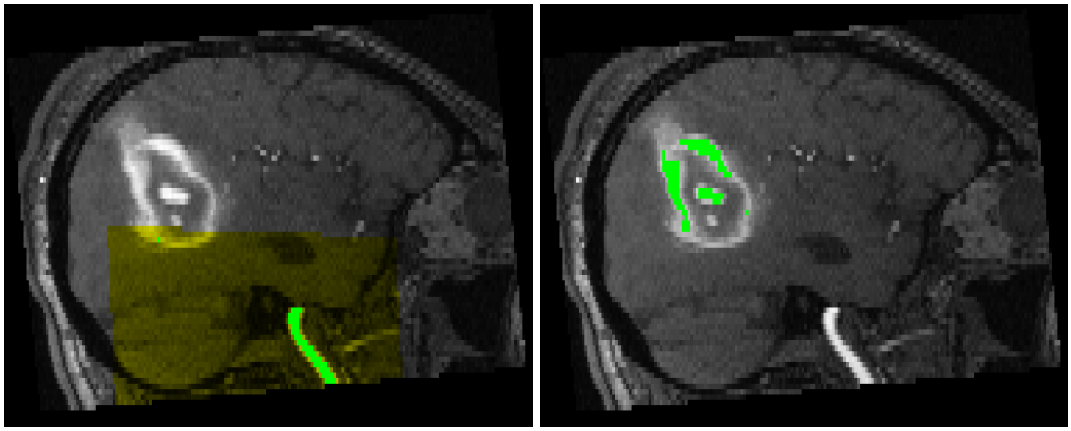

(a) **(b)**

Figure 3.1: Comparison of carotid segmentation (green) with (a) and without (b) a cuboid mask (yellow). In the absence of the cuboid mask, the segmentation algorithm fails to capture the carotid and instead incorrectly identifies the brain lesion

3.2 IDIF

IDIF estimation was performed using both the Bayesian GTM (BGTM) and the GTM PVC method. The average mean absolute error (MAE) of the cAUC across the dataset was 14,202

Metric	BGTM		GTM	
	μ	σ	μ	σ
cAUC MAE	14,202	9,190	33,764	21,212
MR_{glu} MAPE (%)	**14.1**	**10.1**	33.0	31.5
MR_{glu} MAE	1.42	1.07	3.50	3.38
R^2 MAE	0.004	0.006	0.030	0.132
Slope MAE	0.14	0.109	0.304	0.230

Table 3.1: Summary of performance metrics for BGTM and GTM methods.

for BGTM and 33,764 for GTM.

ROI-based quantification was carried out using both IDIFs, with BGTM yielding significantly better performance. BGTM and GTM methods acheived an Average MR_{glu} MAPE of 14.1% and 33%, and an AVERAGE MR_{glu} MAE of 1.42 and 3.5, respectively. Additionally, R^2 MAE and S MAE were 0.004 and 0.14 for BGTM, and 0.030 and 0.304 for GTM, respectively.

As seen in Figure **??**, there is high correlation between the MAE cUAC curve error and the mentioned quantification errors.

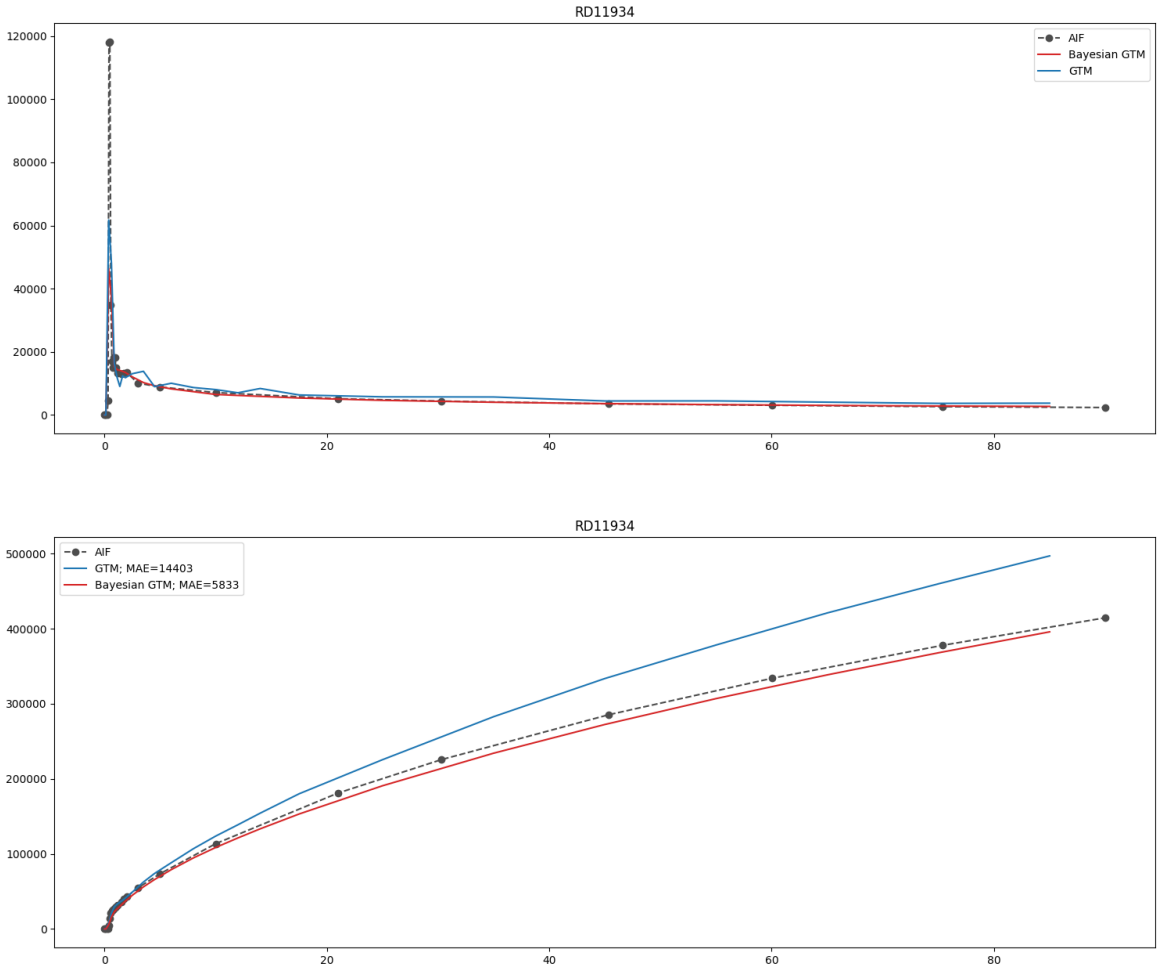

Figure 3.2: Comparison of the IFs (Top) and Cumulative AUC curves (Bottom) for a specific subject

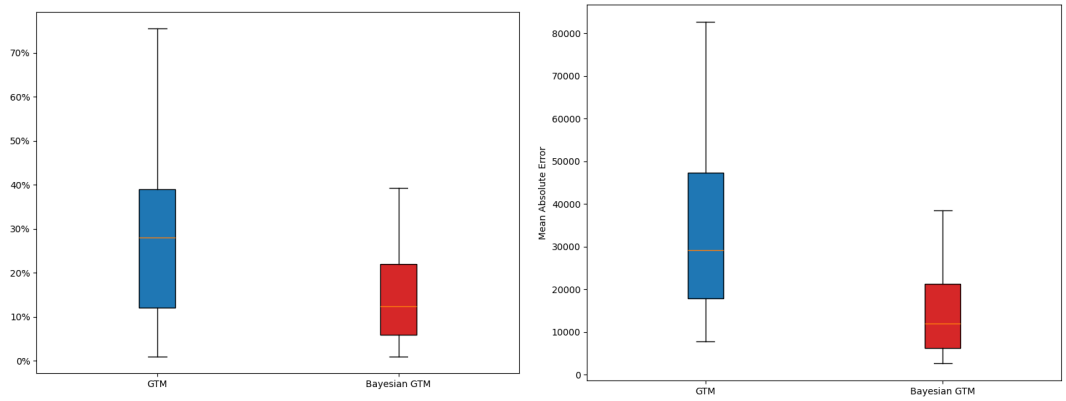

(a) MR_{glu} MAPE Boxplot **(b)** cAUC MAE Boxplot

Figure 3.3: Boxplot of curve and quantification errors

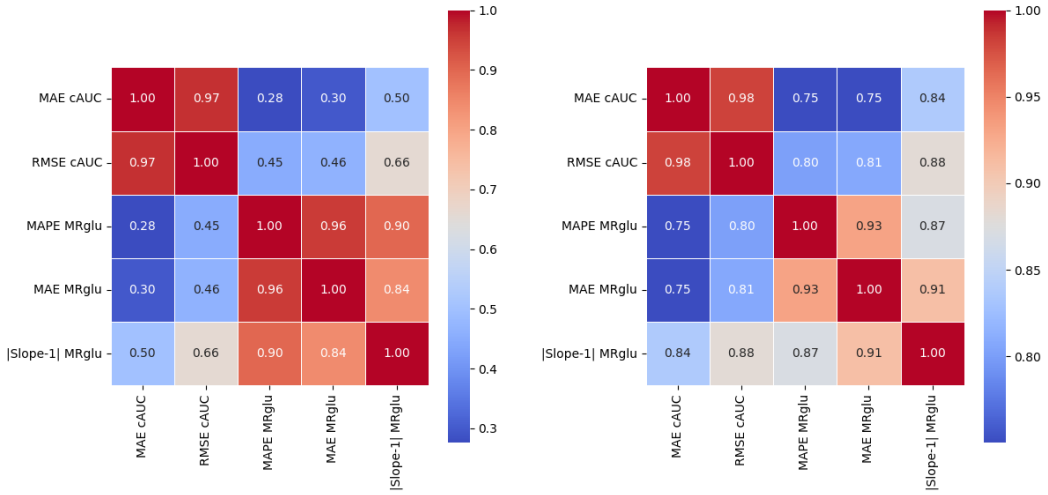

(a) GTM **(b)** Bayesian GTM

Figure 3.4: Correlation matrix of different metrics for Bayesian GTM and GTM methods

Discussion

Conclusion

References

[1] Zacharie Irace et al. “Bayesian partial volume correction for image derived input function”. In: *JOURNAL OF CEREBRAL BLOOD FLOW AND METABOLISM*. Vol. 41. 1_ SUPPL. SAGE PUBLICATIONS INC 2455 TELLER RD, THOUSAND OAKS, CA 91320 USA. 2021, pp. 229–229.

[2] Camille Jouvie. “Estimation de la fonction d’entrée en tomographie par é mission de positons dynamique : application au fluorodesoxyglucose”. Theses. Université Paris Sud - Paris XI, Dec. 2013.

[3] Vesa Oikonen et al. *TPCCLIB*. Version 0.6.20. Retrieved on 2nd February 2025. Turku PET Centre, University of Turku, 2018. URL: `https://gitlab.utu.fi/vesoik/tpcclib`.